A new measuring concept to determine the lift force for distorted bubbles in low Morton number system: Results for air/water

Ziegenhein, T.; Tomiyama, A.; Lucas, D.;

Originally published:

June 2018

International Journal of Multiphase Flow 108(2018), 11-24

DOI: https://doi.org/10.1016/j.ijmultiphaseflow.2018.06.012

Perma-Link to Publication Repository of HZDR:

https://www.hzdr.de/publications/Publ-26508

A new measuring concept to determine the lift force for distorted bubbles in low Morton number system: Results for air/water

T. Ziegenhein[a,*], A. Tomiyama[b], D. Lucas[a]

[a] Helmholtz-Zentrum Dresden-Rossendorf e.V., 01314 Dresden, Germany

[b] Graduate School of Engineering, Kobe University, 1-1, Rokkodai, Nada, Kobe 657-8501, Japan

* Corresponding author. Tel.: +49 3512602503; fax: +49 3512603440.
E-mail address: t.ziegenhein@hzdr.de (Thomas Ziegenhein).

Abstract

The lift force, which strongly influences the spatial bubble distribution, is one of the most important non-drag forces. However, measurements in systems with a low Morton number are limited. In the present work, a time-averaging measurement method with which this gap can be closed is discussed. The experimental setup is kept as simple as possible, avoiding any moving parts. The single bubble movement through a linear shear field was observed three-dimensional over 75 minutes. In total, 85 measurement points cover 13 bubble sizes at 7 different shear rates. The results reveal that former empirical correlations obtained from experiments and simulations in predominantly high Morton number systems are applicable. In this context, the characteristic length scale that is used to describe the lift force needs to be carefully defined. From the present results, the major axis seems to be the most reasonable choice for wobbling bubbles. However, the major axis might be dependent on the flow properties, which leads to a flow dependent lift force formulation.

Keywords

Bubbly flows, Lift coefficient, Wobbling bubbles, Bubble shape

1 Introduction

Bubbly flows play an important role in many industrial production processes, safety engineering, as well as in natural phenomena. Since the bulk flow in such applications is usually non-uniform, so-called non-drag forces strongly affect the flow-structure. As one of the very important non-drag forces, the lift force on bubbles in shear fields is studied intensively since the 70's of the last century. In pipe flows, specifically in the field of nuclear safety engineering, the effect was early noticed by observing gas accumulations near the walls (e.g. by Rouhani (1976)). However, the impact on the flow structure is manifold. In general, the lift force tends to stabilize or destabilize a flow regime, depending on the sign of the lift coefficient (Lucas et al. 2005). Despite its importance, the lift force is yet not well understood; even, reliable measurements are limited under industrially relevant conditions. The present work aims to fill this gap by studying a new measurement concept for low Morton number systems and non-laminar background flows.

For spherical bubbles, the lift force is connected to the lift force of rigid spheres under certain flow circumstances; indeed, for the asymptotical solution of an inviscid bubble in viscid fluids and finite shear rates the lift coefficient is $\left({}^{2}/_{3}\right)^{2}$ times the coefficient of a rigid sphere (Mei & Klausner 1994) (Legendre & Magnaudet 1997). However, the complexity is increased as being away from asymptotic conditions (Legendre & Magnaudet 1998) and hardly describable when the assumption of spherical bubbles is not valid any more.

Kariyasaki (1987) showed that the lift force is different for large, deformable bubbles by using the well-known rotating belt experiments. He was able to demonstrate that large bubbles travel in the opposite direction in a linear shear field compared to small bubbles. This sign change could be reproduced in numerical simulations (e.g. Ervin & Tryggvason (1997), Bothe et al. (2006), and Dijkhuizen et al. (2010)) and experimentally by Tomiyama et al. (2002), Aoyama et al. (2017) as well as by Lucas & Tomiyama (2011). For a systematic description, attempts were made to split the problem in a shear-induced and shape-induced part. For the later, the direct numerical simulations by Naciri (1992) and Adoua (2009) should be noted, who revealed a very complex behavior of the lift force depending on the Reynolds number, aspect ratio and shear rate.

To fulfill the purpose of measuring the lift force for deformable bubbles that are traveling on chaotic paths in low Morton number systems, an averaging procedure is needed. The established method of evaluating the path inclination of single bubbles, which is used for the evaluation of experiments (e.g. Tomiyama et al. (2002)) and for Direct Numerical Simulations (DNS) (e.g. Bothe et al. (2006)), is not applicable. Indirect measurement concepts that are for example proposed by Kulkarni (2008) and Lucas & Tomiyama (2011) are not exact or are not able to quantify the lift force.

The time-averaging procedure and the corresponding force equilibrium described in the present work are feasible for low Morton number systems and turbulent conditions.

Moreover, a very simple experimental setup is used with which a linear shear field can be generated without using moving parts. Finally, the results are critically discussed and compared to previous measurements and simulations.

For the evaluation of the lift force, we use the formulation of Zun (1980) based on the formulation for rigid spherical particles by Lawler (1971)

$$F_{Lift} = -C_L \rho_L (\vec{u}_G - \vec{u}_L) \times rot(\vec{u}_L) \ . \quad (1)$$

Deionized water as the continuous phase and filtered air as the dispersed phase are used. For interpreting and comparing the results to previous work, we use the following set of dimensionless numbers

$$Eo = \frac{\Delta\rho g d_B^2}{\sigma}, Eo_\perp = \frac{\Delta\rho g d_\perp^2}{\sigma}, Re_B = \frac{\rho v_{rel} d_B}{\mu}, Re_\perp = \frac{\rho v_{rel} d_\perp}{\mu}, Mo = \frac{g\mu^4\Delta\rho}{\rho^2\sigma^3} \ . \quad (2)$$

The modified Eötvös $Eo_\perp$ and Reynolds number $Re_\perp$ are calculated with the major axis of the bubble $d_\perp$. All volume flow rates are given at atmospheric pressure, 1.013 bar, and room temperature, 20°C. The measurements cover the following range: $0.62 < Eo < 3.83$, $1.18 < Eo_\perp < 11.1$, $760 < Re_\perp < 2185$, and $Mo = 2.63 \cdot 10^{-11}$.

2 Experimental setup and measuring concept

To simplify the evaluation of the lift coefficient, linear shear fields are in the focus. In low viscid fluids, however, a linear shear field is not easy to create. In particular, shear that is generated at walls hardly creates proper shear fields, which excludes the usage of rotating belts as used in previous measurements. Using pumps to create pressure gradients to drive a flow with a linear shear field is complicated and needs a very elaborate experimental setup. Moreover, pumps and other moving parts can contaminate the fluid due to abrasion and can create undesired oscillations in the system. Moreover, the experimental setup needs a very large amount of fluid due to long running-in distances. To overcome these problems, we drive a circulating flow in a rectangular bubble column by bubbles (Figure 1). An elongated vortex is generated in the whole column by the bubbles generated at one side. Inside the vortex, an almost linear shear field over a wide area is obtained due to the geometry of the column, which was designed by Computational Fluid Dynamics (CFD) simulation beforehand. The lift force is studied with bubbles generated at the opposite side traveling through the linear shear field of the vortex.

We used deionized water that was replaced every four hours. The bubbly flow that drives the fluid was generated with four 0.6 mm needles. For the lift force evaluation, single bubbles were generated using various needles. With this method, bubbles in the range from 2.45 to 6.4 mm diameter of an equivalent volume sphere were constantly generated at gas volume flows up to 11 cm^3/min. The shear rate was varied in the range of 2.1 to 2.8 $1/s$ by varying the gas volume flow rate of the driving bubbly flow from 0.6 l/min to 1.2 l/min. In total, 13 bubble sizes at 7 shear rates were evaluated. However, the results of the highest shear rate

for the six largest bubbles were sorted out since the bubble paths were too close to the driving bubbly flow. Overall, 85 measuring points are taken into account. Per measuring point, the flow was measured five times each 15 minutes with a gap of about 10 minutes in between. The measurements were consecutively conducted over 7 weeks.

In order to correct the perspective of the camera and to evaluate the flow in three dimensions, the bubbles were stereoscopically recorded by using two Red Lake Motion Pro cameras with a 70 mm f3.6 Sigma lens for the front and a 50 mm f1.4 Nikkor lens for the side view. The bubbles were automatically identified by using a modified Canny edge detector. The bubble velocity was determined by tracking the bubbles over 10 pictures. Both methods are described in our previous work (Ziegenhein et al. 2016) in detail. The liquid velocity field was measured with Particle Image Velocimetry (PIV). For this purpose, the flow was seeded with 20-50 µm Rhodamine imprinted PMMA particles from microParticles GmbH. The particles were illuminated by a double-pulsed, two dimensional laser light sheet from the side. The time difference between the pulses was 1/2500 s; the double pulse was generated every 0.2 s. The flow field differed slightly when different bubble sizes for the lift force evaluation were generated at the side so that for all 85 measuring points the liquid velocity field was measured. The bubbles that are traveling through the measurement area were masked for the PIV measurements as described in our previous work (Ziegenhein & Lucas 2016). The bias sampling that occurs due to the presence of bubbles before the measuring plane and due to the shadows of the bubbles in the measuring plane (Ziegenhein & Lucas 2016) was considered but negligibly small. The PIV measurements were executed in an extra step after the bubbly flow measurements so that the single bubbles with which the lift force was measured were not contaminated with the Rhodamine tracer particles.

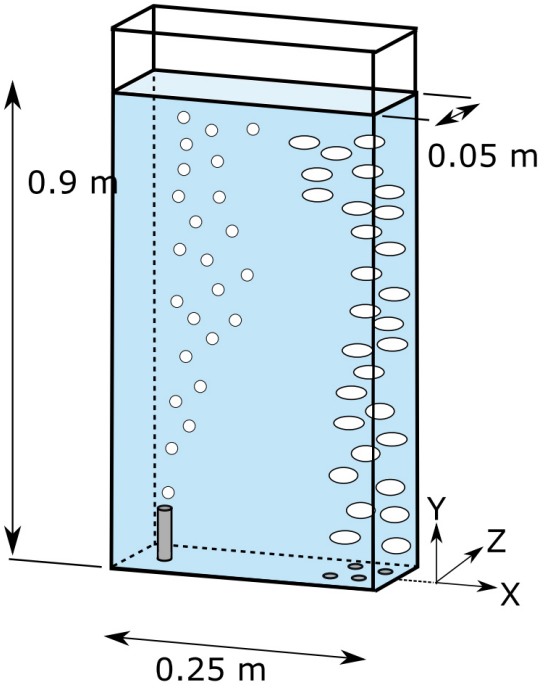

Figure 1 Experimental setup

2.1 Liquid Velocity field

The time averaged liquid velocity field generated by the driving bubbly flow is shown for 0.8 l/min in Figure 2. The bubbles for the lift force evaluation, which are generated at the left side of the column, rise up through the downward flow section of the elongated vortex. The driving bubbly flow on the right side generates a constant shear field with respect to the vertical liquid velocity at different heights. Due to the nature of the vortex, however, the horizontal velocity is not constant over height. The horizontal liquid velocity is crucial for the horizontal slip velocity and will be taken into taken account for the lift force evaluation.

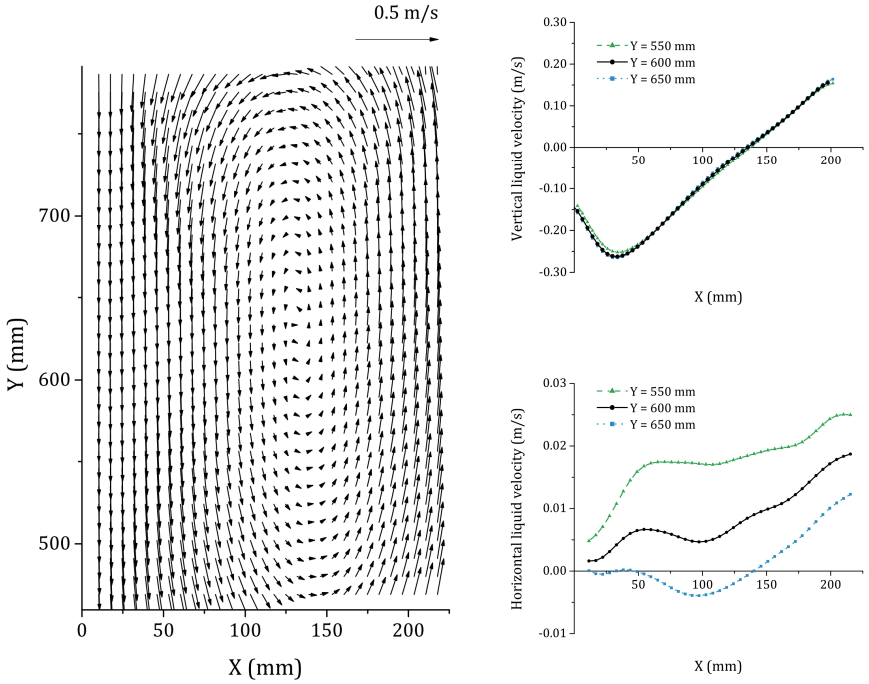

Figure 2 Liquid velocity field in the center of the column for a gas volume flow of the driving bubbly flows of 0.8 l/min.

Important for the evaluation of the lift force is a flat velocity profile in depth. On one hand, it simplifies the force balance since the depth direction can be neglected when a time average is applied. On the other hand, it is vital to guarantee that bubbles do not cluster at certain positions. For example, when a center-peaked downward velocity profile is present, large bubbles with a negative lift coefficient would be pushed to the wall due the lift force. Consequently, asymmetrical wall effects disturb the wake structure distinctly and as a result, no meaningful measurement would be possible. By shifting the PIV measurement step-by-step out of the center (Figure 3) a sufficiently flat liquid velocity profile was proven.

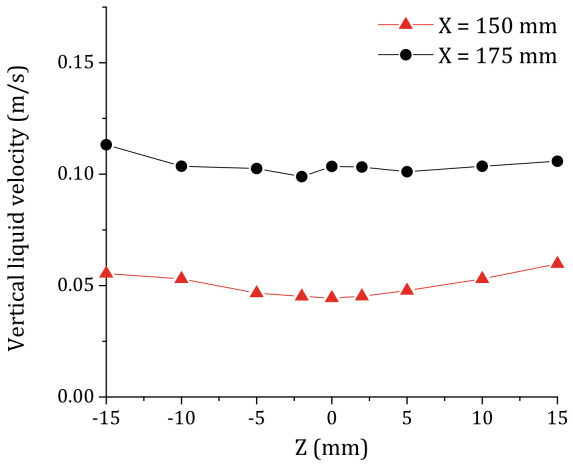

Figure 3 Liquid velocity profiles in depth direction at two different Position at a height of Y=600 mm.

The turbulence is moderate and linearly increasing with increasing flow rates of the driving bubbly flow. The turbulent kinetic energy (Figure 4) is determined by the free surface of the bubble column and the driving bubbly flow. Moreover, local differences can be observed with a minimum in the center of the vortex and an anisotropic behavior in the downward flow region.

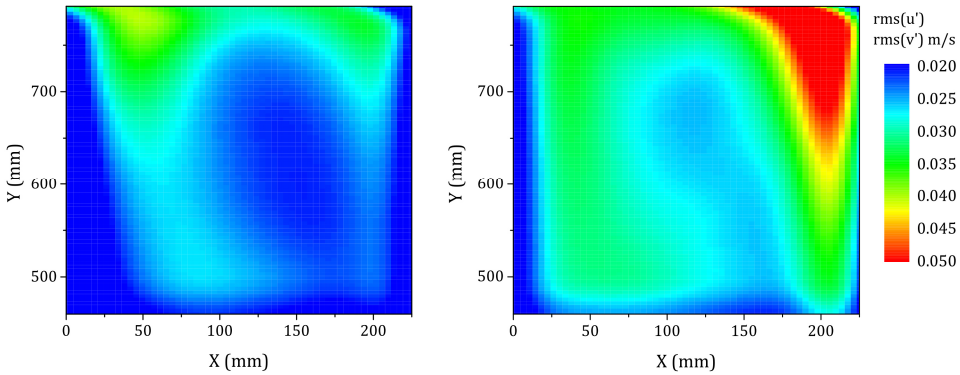

Figure 4 Root mean square (rms) of the two normal fluctuation components u' (horizontal direction) and v' (vertical direction) for a gas volume flow of the driving bubbly flow of 0.8 l/min.

2.2 Bubble Generation

The bubbles for the lift force evaluation were generated with needle spargers and a mass flow controller including a control unit to maintain a constant gas volume flow. To constantly generate large bubbles, plastic caps in which the bubbles coalesced before leaving the sparger were used. This method is relatively simple but can produce a wider bubble size distribution due to transient instabilities. However, because of the long measurement time and the needed large amount of bubbles a mechanical bubble generator was not applicable. Despite outliers were identified based on the diameter of an equivalent volume sphere

(Figure 5 left), the major axis distribution is still very wide (Figure 5 right) due to wobbling effects. The major axis in this work is defined as the longest axis of the bubble projected on the front view, which is substantially larger than the horizontal axis for wobbling bubbles. Previous work under laminar conditions used the perpendicular axis to the flow. However, under laminar conditions the major axis, the perpendicular axis to the flow and the horizontal axis are equivalent since the bubbles are not wobbling or meandering. In turbulent conditions, the instant perpendicular axis to the flow is not known and the perpendicular axis to the time averaged flow as well as the horizontal axis is not meaningful. Under the assumption that the major axis and the instantaneous perpendicular axis to the flow are similar, we decided to use the major axis as a dominant length scale. This choice is supported by a very good agreement between the present results and previous work as will be discussed in the result section.

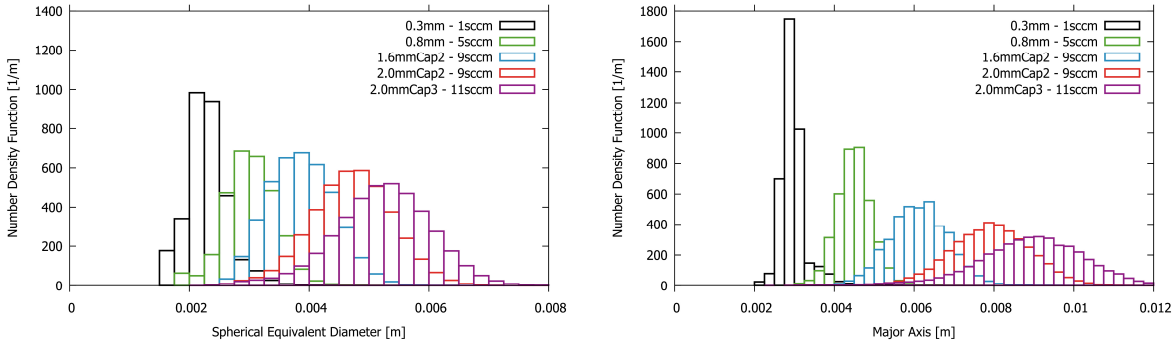

Figure 5 Bubble size distribution (left) and major axis distribution (right) for different sparger sizes and setups.

2.3 Gas phase velocity

The gas phase velocity is determined by tracking the bubble center. The bubbles were recorded and tracked in sets of 10 successive pictures recorded with 250 frames per second with a gap of 1 second between the sets. The time-averaged results are illustrated in Figure 6. As a first impression from the vector plots, the shear field of the liquid velocity can be nicely observed and the small bubbles of 2.97 mm size ($C_L = 0.28$) tend to move to the left side whereas the larger bubbles of 4.23 mm size ($C_L = -0.01$) are traveling more or less straight upwards. For evaluating the lift force, the bubble velocity was determined only along the averaged path, which is described in the next section. The mapping on a mesh shown in Figure 6, which is just for illustrations, was not used.

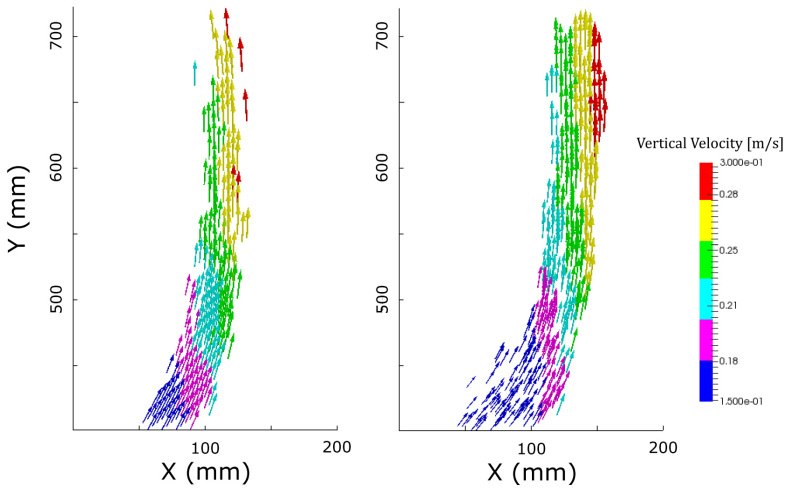

Figure 6 Illustrated time averaged bubble velocity for 2.97 mm bubbles (left) and 4.27 mm bubbles (right) for 0.8 l/min gas volume flow of the driving bubbly flow.

Knowing the bubble velocity and the liquid velocity field, the vertical slip velocity can be calculated easily (Figure 7). The results fall on the semi-empirical correlation of Bozzano & Dente (2001) that was formulated for clean conditions. Since the slip velocity would be smaller the more the flow is contaminated (Ishii & Zuber 1979), the results indicate that the deionized water used was sufficiently clean.

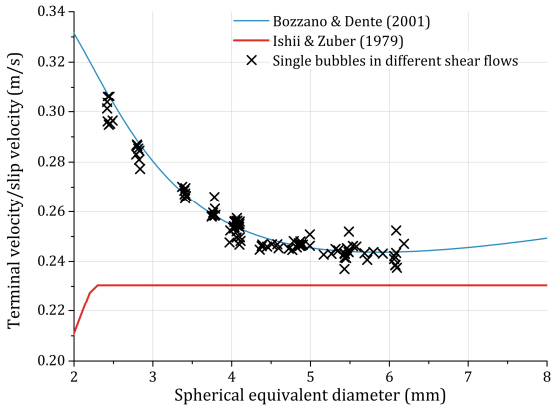

Figure 7 Measured slip velocity of the bubbles in vertical direction compared to the terminal velocity calculated from different models.

2.4 Path averaging

Wobbling bubbles under non-laminar conditions have chaotic pathways through a more or less chaotic turbulent shear field. Since the flow field around the bubble is hardly measureable, an averaging procedure has to be applied. A suitable averaging framework is the two-fluid approach of Ishii & Hibiki (2006). The gas phase and the liquid phase are modeled as interpenetrating continua represented with a void fraction. The resulting momentum equations can be solved numerically on a grid. This procedure is the basis for determining the lift coefficient in the present work. The void fraction, liquid velocity, and gas

phase velocity field are measured. Under the assumption of negligible pressure forces on the gas phase the force equilibrium on the averaged gas phase is zero so that the lift force can be calculated.

The void fraction field is determined three-dimensionally in the measuring volume. For this purpose, an isotropic grid with a distance from point to point of 0.1 mm is used, resulting in a 30 million-cell grid. On this grid, every measured bubble is represented by a three-dimensional ellipsoid including the bubble's inclination. If a grid point is inside a bubble, a counter on this point is increased by one. After dividing the counter by the amount of pictures taken, a representative three-dimensional void fraction is obtained. An isosurface of the resulting ensemble averaged void fraction, which is equal to a time-averaging procedure, is shown in Figure 8.

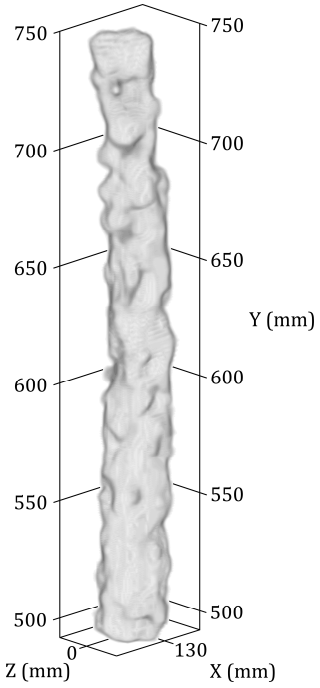

Figure 8 Isosurface at $\alpha/\alpha_{max} = 0.46$ of the three-dimensional void fraction for a bubble size of 2.97 mm and a driving bubbly flow of 0.8 l/min.

In order to formulate a reasonable force balance equation, the maximum void fraction path is searched. This path is the connection of the maxima in different horizontal *xz*-slices along the *y*-axis. For this purpose, the three-dimensional mesh was coarsen by averaging over 10x10x10 cells resulting in a 1 mm grid size. The maxima were afterwards connected through a spline interpolation to get a reasonably smooth path.

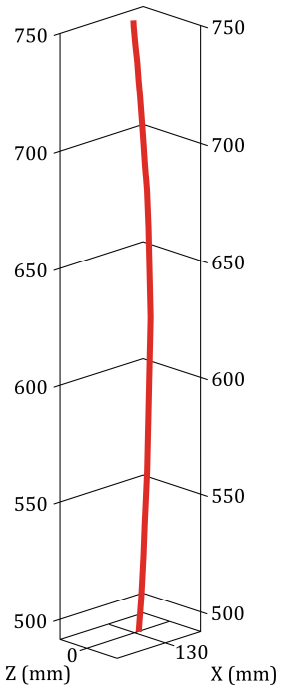

Figure 9 The averaged bubble path obtained from the three-dimensional void fraction shown in Figure 8.

2.5 Calculating the lift coefficient

The necessary set of forces in the framework of the time averaging procedure (indicated with a bar over the variables) needs to be defined at first. In this context, we consider the buoyancy force, the virtual mass, the drag, the wall, and the turbulent dispersion forces; other effects like the Basset force or turbophoresis are neglected. In spite of this relatively simple set of forces, some assumptions need to be made. At first, the turbulent dispersion force is up to now not well defined, different models can be found in literature that take different effects into account. However, regarding the time averaged turbulent dispersion force all formulations depend on the spatial gradient of the void fraction. The turbulent dispersion force therefore does not need to be considered along the maximum void fraction path since it is connecting the time averaged local maxima. Hence, the first assumption can be written as:

$$\overline{F_{TurbDisp}\left(u_L(t), d_B(t)\right)}\Big|_{\frac{d\alpha}{dx_i}=0} = 0 \ . \tag{3}$$

Since the maximum void fraction path is in the center of the column, the wall forces do not need to be considered. Further, we assume that the model coefficients of the forces are (time averaged) isotropic, except for the virtual mass force coefficient, which is in line with previous lift force measurements. Next, we assume that the slip velocity is not correlated to moderate shear rates, which was shown by Dijkhuizen et al. (2010) by Direct Numerical Simulations (DNS). This assumption can be written as:

$$\overline{\frac{du_L}{dx}|u_G - u_L|} = \overline{\frac{du_L}{dx}}\ \overline{|u_G - u_L|}\ . \tag{4}$$

Last, we assume a weak correlation between the model coefficients and the flow parameters. This is commonly used in all two-phase simulations that include an averaging or filtering process for turbulence. Looking at the lift force formulation in one direction, the averaging process for a constant liquid density is written as

$$\begin{aligned}\overline{C_L\left(\vec{u}_{G,y} - \vec{u}_{L,y}\right) \cdot \frac{du_{L,y}}{dx}} \\ = Cov\left(C_L, \left(\vec{u}_{G,y} - \vec{u}_{L,y}\right) \cdot \frac{du_{L,y}}{dx}\right) \\ + \overline{C_L}\left(Cov\left(\left(\vec{u}_{G,y} - \vec{u}_{L,y}\right), \frac{du_{L,y}}{dx}\right) + \overline{\left(\vec{u}_{G,y} - \vec{u}_{L,y}\right)}\ \overline{\frac{du_{L,y}}{dx}}\right),\end{aligned} \tag{5}$$

with Cov the Covariance. Using the assumption from Equation (4), this can be rewritten as

$$\begin{aligned}\overline{C_L}\left(\overline{\vec{u}_{G,y}} - \overline{\vec{u}_{L,y}}\right)\overline{\frac{du_{L,y}}{dx}} \\ = \overline{C_L\left(\vec{u}_{G,y} - \vec{u}_{L,y}\right) \cdot \frac{du_{L,y}}{dx}} - Cov\left(C_L, \left(\vec{u}_{G,y} - \vec{u}_{L,y}\right) \cdot \frac{du_{L,y}}{dx}\right)\ .\end{aligned} \tag{6}$$

With the assumption of a weak correlation between the lift coefficient and the product of the slip velocity and shear rate, the covariance term is zero and the averaged lift force is equal to the lift force calculated from the single time averaged components.

The assumptions made simplify not only the force formulation, but also the measurements. In particular, the gas and liquid phase properties can be measured separately. Overall, the force balance that is used along the bubble path can be written as:

$$\begin{aligned}\overline{C_L}\rho_L\left(\overline{\vec{u}_G} - \overline{\vec{u}_L}\right) \times rot\left(\overline{\vec{u}_L}\right) \\ = \Delta\rho\vec{g} + \boldsymbol{C_{VM}}\rho_L\frac{D\overline{\vec{u}_L}}{Dt} + \frac{3}{4}\frac{1}{\overline{d_B}}\ C_D\rho_L\left|\overline{\vec{u}_G} - \overline{\vec{u}_L}\right|\left(\overline{\vec{u}_G} - \overline{\vec{u}_L}\right).\end{aligned} \tag{7}$$

The virtual mass coefficient, $\boldsymbol{C_{VM}}$, is an anisotropic tensor with only values different from zero on the main diagonal. The values for $\boldsymbol{C_{VM}}$ are calculated as suggested by (Tomiyama 2004), which were close to 0.5. The drag coefficient, C_D, is taken from the correlation of Bozzano & Dente (2001).

The force balance is only applicable along the averaged path obtained from the three-dimensional void fraction. The local lift coefficient is now simply calculated from Equation (7). For this purpose, the liquid velocity determined in the interrogation areas of the PIV discretization is interpolated to the path positions. The gas phase velocity as well as the bubble size is calculated by a weighted average in a 5 mm sphere around the path positions. The time-averaged values are determined by averaging over all bubbles inside this sphere.

The weight for averaging inside the sphere, which is defined between 0.2 and 1, is the distance to the path position; the closer the bubble is to the path position the higher the weight.

3 Results

3.1 Local results

Solving the force balance from Equation (7), the lift force can be determined locally along the averaged path. Examples of these paths with a representation of the slip velocity are shown in Figure 10 a) for three different bubble sizes. The examples have a positive, vanishingly small, and negative lift coefficient, which can be clearly seen from the slip velocity vectors pointing in different directions. The slip velocity in horizontal direction (Figure 10 b)) is the crucial component for calculating the lift coefficient (Figure 10 c)). The shear rate du_y/dx (u_y is the liquid velocity in vertical direction and x the horizontal coordinate), which causes a horizontal lift force, is dominant compared to du_x/dy (Figure 10 d)). The other shear rates are a factor of 100 smaller than du_y/dx.

The slip velocity in horizontal direction is small compared to the slip velocity in vertical direction, which demands a high resolution of the determined liquid and bubble velocity. The wobbling of the bubbles causes a very high instantaneous horizontal velocity, which is the reason for the very long measuring time. The measuring time is further increased because the time-averaged bubble velocities required for force equilibrium, Eq. (7), are obtained by averaging the instantaneous velocities of bubbles near the averaged path. Therefore, measured bubbles away from the path, which are the majority, are not considered. All in all, the measurement of a small slip velocity from a high fluctuating bubble velocity and the usage of two different measurement methods for the bubble velocity (PTV) and liquid velocity (PIV) at separated times, are the key points of the present method. In general, the used measuring time is not sufficient to resolve locally the lift force, which is indicated by the fluctuating lift coefficient over height in Figure 10 c). Averaging the results along the path improves the statistics and meaningful results are obtained.

Wobbling bubbles rise in quiescent water in more or less stable pathways, which can substantially influence the forces acting on them (Tomiyama 2004). When the background flow was not present, this behavior of bubbles rising in chains was also observed for the time averaged bubble paths. However, with the turbulent background flow, pattern-like steady oscillations in the bubble paths, slip velocities, and lift coefficient results were not observed. Therefore, it can be assumed that the bubbly flow is truly random and the averaging process is reasonable.

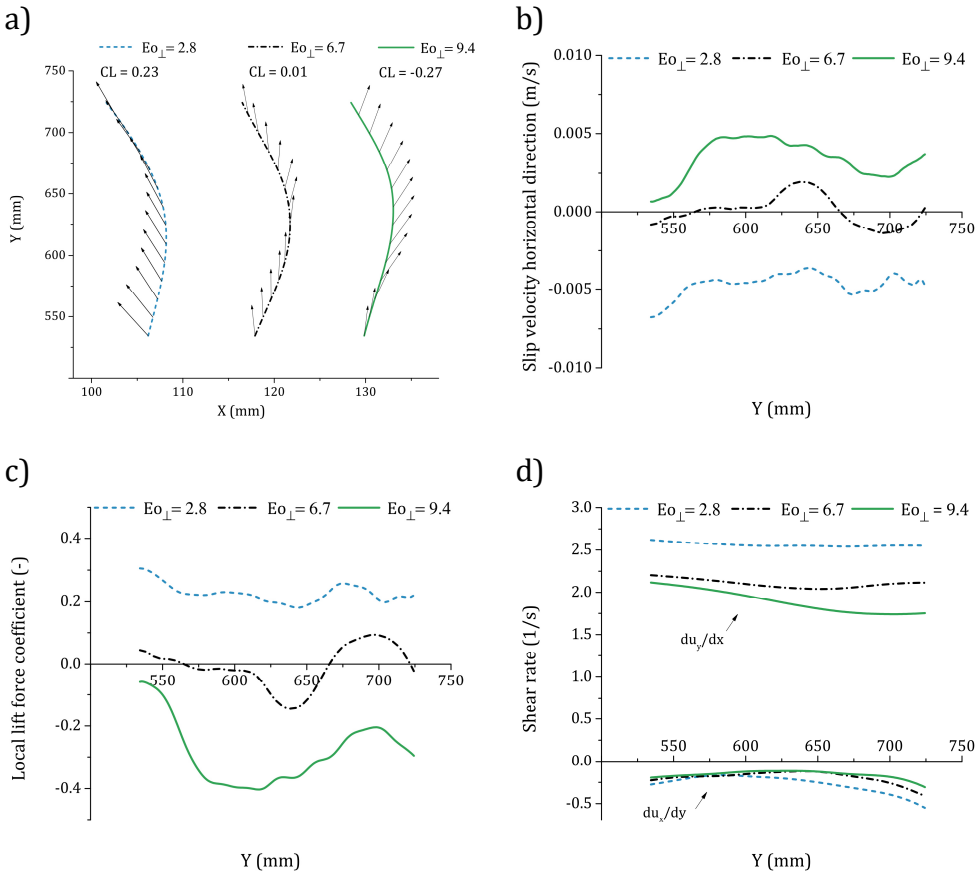

Figure 10 Results along averaged bubble paths for three bubble sizes. a) The averaged path with the slip velocity as vector, for a better representation the x component of the slip velocity was multiplied by 5. b),c),d) The slip velocity in x-direction, the local lift coefficient and the shear rate, respectively, on the averaged path with the y-coordinates as parameter.

3.2 Shear rate dependency and reproducibility

By varying the gas volume flow rate of the driving bubbly flow, seven different shear rates were investigated in the range of 2.1 and 2.8 $1/s$ (Figure 11). The measurements of Tomiyama et al. (2002) under laminar conditions and for high Morton numbers revealed no dependency on the shear rate. DNS in lower Morton number systems (Dijkhuizen et al. 2010) likewise revealed no dependency on the shear rate. However, the DNS results scatter too much for a definite statement. Recent measurements of Aoyama et al. (2017) show a slight dependency for Reynolds numbers below 10. A clear dependency of the lift coefficient on the shear rate was also not observed in the present experiments with Reynolds numbers around 1000. Nonetheless, the present results tend to scatter too so that a trend might be covered in the statistical uncertainty.

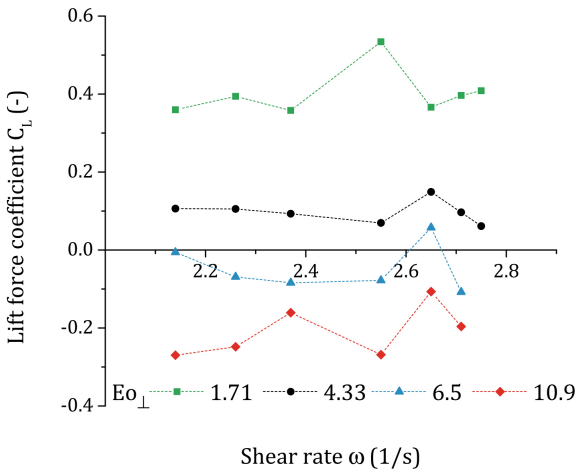

Figure 11 Lift force results for different shear rates and different major axes.

If no dependency of the lift coefficient on the investigated shear rates is assumed, the results for the same bubble sizes can be used to assess the reproducibility of the experiments. For this purpose, we excluded extreme outliers like the result for $Eo_{\perp} = 1.71$ at a shear rate at around $2.575\ 1/s$ shown in Figure 11; however, only one outlier per bubble size was excluded. Such outliers are caused by the long time measurement campaign of seven weeks and that almost all data points shown in Figure 11 are obtained at different days. Even with great care and a daily calibration of the setup, operational errors or other trivial errors are hardly avoided over a 35 days measurement campaign that need to be very exactly executed.

In Figure 12, the results are shown with respect to the Eötvös number calculated with the diameter of an equivalent volume sphere as length scale. While the six single measurements for smaller bubbles lie close together, the results scatter very much for the larger bubbles. This large scatter is simply caused by insufficient statistics. While we tracked 60,000 bubbles of the smallest bubble size in the 75 minutes measuring time per measuring point, we tracked only 4,000 bubbles for the largest bubble size. The reason for this smaller bubble count is that the bubble diameter is increasing with the cube root regarding the bubble volume. However, the gas flow rate was limited since we observed during the PIV measurements a distinct influence on the vortex structure when large bubbles at relatively high frequencies were generated.

To assess the repeatability over the complete measuring campaign, we measured the lift coefficient around $Eo = 1.75$ three times with different sparger setups at the beginning, in the middle and the end of the campaign. The 18 measuring points are reasonably close together in Figure 12 so that it can be assumed that the measuring conditions like water quality were not changing. Further, to determine the sign change of the lift force, two measurements were executed at the expected Eötvös number of around 2.4.

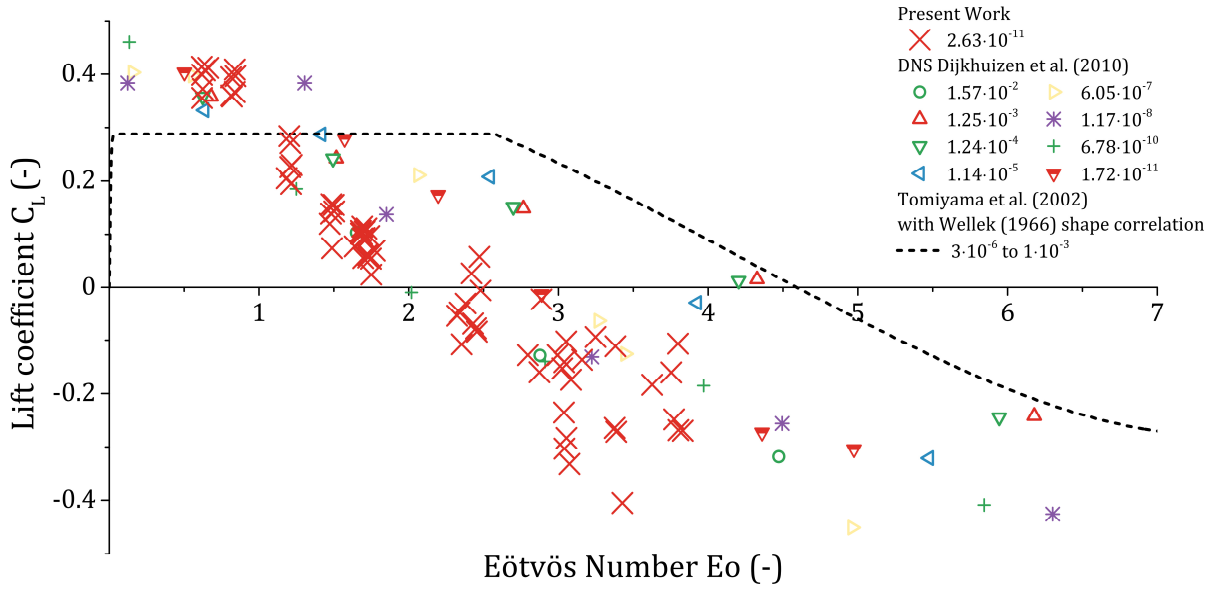

Figure 12 Results of the lift force measurements compared to results from literature for different Morton numbers. For the Tomiyama correlation, the Wellek (1966) correlation is used to calculate the spherical equal bubble size for their system of glycerol-water mixtures.

3.3 Comparison to the literature

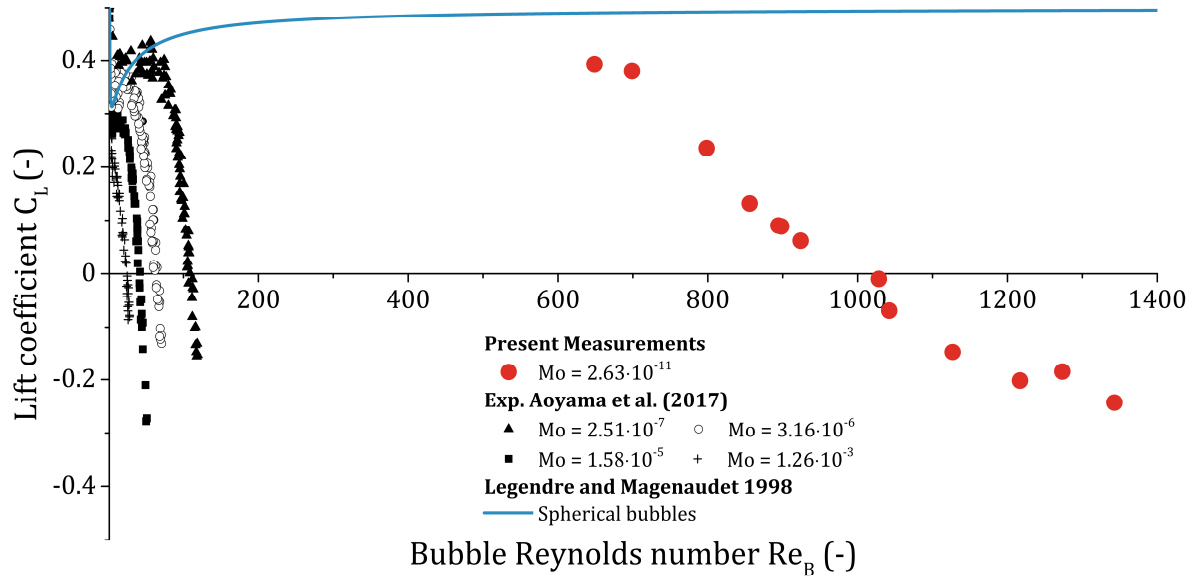

Figure 13 Comparison of the present results with literature with respect to the bubble Reynolds number.

For the further evaluations, the results are averaged over the different shear rates since no dependency of the shear rate is expected as discussed in the previous section. In particular, this averaging helps to increase the statistics for the large bubbles.

A dependency of the lift coefficient of the used system is clearly observable in Figure 12. This dependency is underlined in Figure 13 by comparing the present results to the results of Aoyama et al. (2017) with respect to the bubble Reynolds number. With a decreasing Morton number, the flow around the bubbles becomes more and more turbulent. While Aoyama et al. observed the sign change for the lift force around a Reynolds number of 150 for $Mo = 2.51 \cdot 10^{-7}$, the sign change from the present measurement is already around 1000 for $Mo = 2.63 \cdot 10^{-11}$. However, similarities can be clearly seen. The lift coefficient seems to be linearly changing around the sign change with the Reynolds number. Moreover, the measurements seem to approach the spherical bubble model of Legendre & Magnaudet (1998) for positive lift coefficients. This might be the reason why we do not see a plateau in our measurements at small Eötvös numbers as observed by Tomiyama et al. (Figure 14). The smallest bubbles in our measurements at $Mo = 2.63 \cdot 10^{-11}$ are simply still too deformed to reach the spherical bubble regime; Tomiyama et al., however, reached this limite in their low Morton number experiments.

In addition to the dependency of the Reynolds number, the disagreement of the different lift force measurements in Figure 12 is caused by a complex correlation of the major axis and the used system. Bubbles with the same Eötvös numbers have a different major axis at different Morton numbers. The major axis, however, might be strongly connected to the lift force. If the modified Eötvös number, which is calculated with the major axis as the length scale, is used the agreement between the present measurements, the measurements of Tomiyama et al. and the DNS of Dijkhuizen et al. is good (Figure 14). It should be noted that only the horizontal axes from the DNS of Dijkhuizen et al. and the experiments of Tomiyama et al. are known and it is assumed that the horizontal axis is equal to the major axis at this point. This assumption is reasonable for the experiments of Tomiyama et al. since no wobbling at the combinations of Morton and Eötvös numbers they used occur. However, in the systems used for the DNS, wobbling or path instabilties are likely so that the major axis is underestimated by the horizontal axis, which might be the reason for the general underestimation of the DNS results in Figure 14.

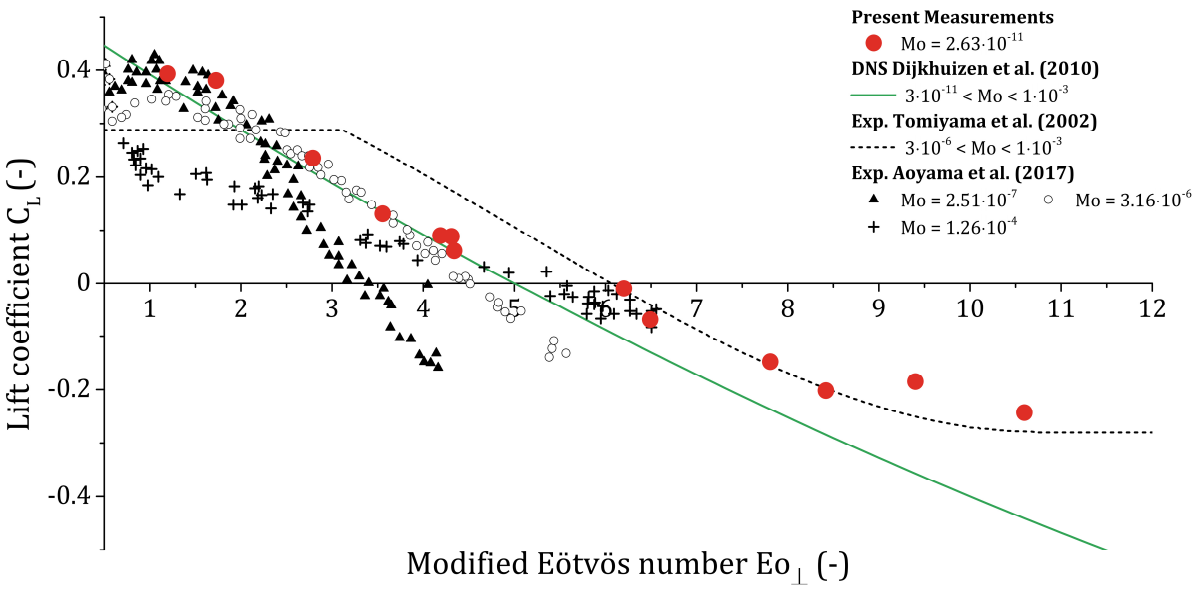

Figure 14 Comparison of the present results with correlations from literature.

The measurements of Aoyama et al. revealed a complex behavior of the lift coefficient regarding the Morton number with respect to the modified Eötvös number. The slope and the sign change are changing distinctly when the Morton number is varied. It seems that the sign change is moving to smaller bubble sizes with decreasing the Morton number. However, this trend is reversed somewhere between $Mo = 2.51 \cdot 10^{-7}$ and $Mo = 2.63 \cdot 10^{-11}$ since our results show a sign change at $Eo_{\perp} \approx 6.1$. As discussed by Aoyama et al. (2017), the findings of Lucas and Tomiyama (2011), who determined the sign change in steam/water systems, support that this upward trend is going on for Morton numbers lower than $Mo = 2.63 \cdot 10^{-11}$. Nevertheless, all lift force measurements show a strong linear trend around the sign change, which might be also the most interesting area for engineering applications.

The steadily descending trend of the lift force with increasing $Eo_{\perp}$ seems to be flatten out for the larger bubbles. However, besides that the statistics for the large bubbles are not satisfactory, a certain wall influence for the large bubbles should be considered at this point. With a major axis of almost 10 mm for the largest bubble, a 50 mm deep test facility might not be sufficient to assume negligible wall effects on the wake structure. Nevertheless, the same behavior of a flat trend of the lift coefficient for larger bubbles after a steep descend was observed in the experiments by Dijkhuizen et al. (2010) in contaminated water, too.

4 Discussion and Conclusions

An averaging procedure to determine the lift force for low Morton systems and turbulent conditions is discussed in the present work. This procedure was applied to single bubbles ascending in a linear shear field created by a bubbly flow in a bubble column. Such a 'bubble pump' setup has the advantage that no moving parts are required and therefore a very

simple measurement concept is obtained. Further, the buoyancy of the bubbly flow is a volumetric force with which sufficiently strong linear shear fields in low viscosity systems can be produced. In total, 85 measuring points are considered for 13 bubble sizes in the range of 2.45 to 6.4 *mm* equivalent volume sphere diameter and 7 shear rates in the range of 2.1 to 2.8 $1/s$.

The results show a clear dependency of the lift force with the bubble size in low Morton number systems under turbulent flow conditions. A dependency of the shear rate on the lift coefficient was not found. Taking the major axis of the bubbles as characteristic length, the results agree very well with the results obtained by Tomiyama et al. (2002) in highly viscous systems and the results of the DNS of Dijkhuizen et al. (2010). The results of Aoyama et al. (2017) reveal a complex connection of the lift coefficient and the Morton number. Nevertheless, the major axis as the characteristic length scale for the lift force phenomena seems to be a reasonable choice.

Since the diameter of an equivalent volume sphere is used to describe the bubble forces, a model for the major axis is needed. For this purpose, the existing aspect ratio correlations can be used if a rotational ellipsoid for the bubble shape is assumed. For example, Tomiyama et al. used the correlation of Wellek et al. (1966) for contaminated systems. In our previous work (Ziegenhein & Lucas 2017) we examined the bubble shape of six different bubble column setups under different flow conditions. We found that the Wellek correlation is underpredicting the major axis for clean air/water system under realistic conditions. Our and the Wellek correlation are compared with the present results by using the formulation

$$d_{\perp} = d_B \sqrt[3]{1 + A\, Eo^B}\,, \tag{8}$$

in Figure 15. As expected, the Wellek correlation underpredicts the major axis, but also our correlation obtained with the same water quality still underpredicts the present results. A reason for this deviation is that we found in our previous work (Ziegenhein & Lucas 2017) a slight flow dependency of the bubble shape, especially for smaller bubbles. Our correlation might be suitable for bubble columns at medium void fractions, but not for single bubble experiments. A proper fit to the present setup with linear shear fields would be obtained with $A, B = 0.7$.

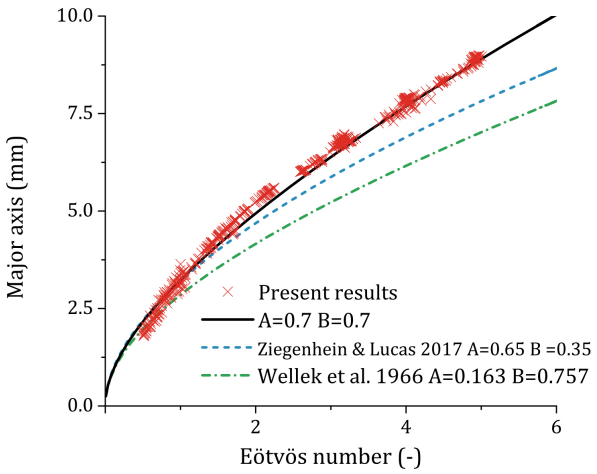

Figure 15 Relation between the Eötvös number and major axis with respect to Equation (10)

The small differences in the bubble shape are crucial for the lift force, in particular for the sign change. The Wellek correlation would predict a sign change around 5.8 mm diameter of an equivalent volume sphere. Our correlation for bubble columns under operating conditions around 5.2 mm. In fact, the present results deliver a sign change at 4.8 mm. By considering an influence of the flow field on the bubble shape, the lift force is indirectly dependent on the flow. In pipe flows with strong gradients, the bubble shape might be even locally changing resulting in complex modelling issues. In this context, a lift force correlation formulated with the modified Eötvös number and a bubble shape correlation obtained under relevant conditions is up to now the most reasonable choice.

The present results are in particular vital for the model development of numerical simulations since a great number of validation experiments are executed in air/water. For such work, the regime in which the lift force correlation is obtained should be evaluated by considering the Reynolds number. Specifically, the plateau of constant lift coefficients, as for example predicted by the Tomiyama correlation, is reached in low Morton number systems at far smaller Eötvös numbers than usually assumed.

Overall, the proposed method for the lift force measurement in turbulent conditions produced reasonable results. Due to the simplicity, this setup might be used for difficult to handle systems since it has no moving parts and does need only a small amount of fluid. In future studies the thickness of the setup will be enlarged to measure larger bubble sizes. Further, the measuring time for large bubbles will be increased to improve the statistics. To get a complete picture of the lift force, further measurements should be executed to close the gap between the present measurements with $\log Mo \approx 11$ and the measurements of Aoyama et al. with a Morton number up to $\log Mo \approx 6.6$, which can be realized with the present setup.

5 References

Adoua, R., Legendre, D. & Magnaudet, J., 2009. Reversal of the lift force on an oblate bubble in a weakly viscous linear shear flow. J. Fluid Mech., Volume 628, p. 23.

Aoyama, Hayashi, K., Hosokawa, S., Lucas, D., Tomiyama, A., 2017. Lift force acting on single bubbles in linear shear flows. International Journal of Multiphase Flow, Volume 96, pp. 113-122.

Besagni, G. & Inzoli, F., 2016. Bubble size distributions and shapes in annular gap bubble column. Exp Therm Fluid Sci, Volume 74, pp. 27-48.

Bothe, D., Schmidtke, M. & Warnecke, H.-J., 2006. VOF-Simulation of the Lift Force for Single Bubbles in a Simple Shear Flow. Chem. Eng. Technol., Volume 29, p. 1048.

Bozzano, G. & Dente, M., 2001. Shape and terminal velocity of single bubble motion: a novel approach. Computers and Chemical Engineering, Volume 25, p. 571–576.

Dijkhuizen, W., van Sint Annaland, M. & Kuipers, J. A., 2010. Numerical and experimental investigation of the lift force on single bubbles. Chemical Engineering Science, Volume 65, p. 1274–1287.

Ervin, E. A. & Tryggvason, G., 1997. The Rise of Bubbles in a Vertical Shear Flow. J. Fluids Eng., Volume 119, p. 443.

Hibiki, T. & Ishii, M., 2007. Lift force in bubbly flow systems. Chemical Engineering Science, Volume 62, p. 6457–6474 .

Ishii, M. & Hibiki, T., 2006. Thermo-Fluid Dynamics of Two-Phase Flow. 2nd ed. New York: Springer Science+Business Media, Inc..

Ishii, M. & Zuber, N., 1979. Drag Coefficient and Relative Velocity in Bubbly, Droplet or Particulate Flows. AlChE Journal, Volume 25, p. 843.

Kariyasaki, A., 1987. Behavior of a single gas bubble in a liquid flow with a linear velocity profile. , Proceedings of the 1987 ASME/JSME Thermal Engineering Conference. No. 384.

Kulkarni, A. A., 2008. Lift force on bubbles in a bubble column reactor: Experimental analysis. Chemical Engineering Science, Volume 63, pp. 1710-1723.

Lawler, M. T., 1971. The role of lift in the radial migration of particles in a pipe flow. Advances in Solid–Liquid Flow in Pipes and Its Application, pp. 39-57.

Legendre, D. & Magnaudet, J., 1997. A note on the lift force on a spherical bubble or drop in a low-Reynolds-number shear flow. Phys. Fluids, Volume 9, p. 3572.

Legendre, D. & Magnaudet, J., 1998. The lift-force on a spherical bubble in a viscous linear shear flow. J. Fluid Mech., Volume 368, p. 81.

Liu, L., Yan, H. & Zhao, G., 2015. Experimental studies on the terminal velocity of air bubbles in water and glycerol aqueous solution. Exp. Therm. Fluid Sci., Volume 62, pp. 109-121.

Lucas, D., Prasser, H.-M. & Manera, A., 2005. Influence of the lift force on the stability of a bubble column. Chemical Engineering Science, Volume 60, p. 3609 – 3619.

Lucas, D. & Tomiyama, A., 2011. On the role of the lateral lift force in poly-dispersed bubbly flows. International Journal of Multiphase Flow, Volume 37, p. 1178.

Mei, R. & Klausner, J., 1994. Shear lift force on spherical bubbles. International Journal of Heat and Fluid Flow, Volume 15, p. 62.

Mougin, G. & Magnaudet, J., 2002. The generalized Kirchhoff equations and their application to the interaction between a rigid body and an arbitrary time-dependent viscous flow. International Journal of Multiphase Flow, Volume 28, p. 1837.

Naciri, A., 1992. Contribution a l'etude des forces exerc´ees par un liquide sur une bulle de gaz: portance, masse ajout´ee et interactions hydrodynamiques. Ec. Centrale Lyon, France. These de Doctorat.

Rouhani, Z., 1976. Effect of wall friction and vortex generation on the radial distribution of different phases. International Journal of Multiphase Flow, 3(1), pp. 35-50.

Tomiyama, A., 2004. Drag, lift and virtual mass forces acting on a single bubble. Pisa, Italy, 3rd International Symposium on Two-Phase Flow.

Tomiyama, A., Kataoka, I., Zun, I. & Sakaguchi, T., 1998. Drag Coefficients of single bubbles under normal and micro gravity conditions. JSME International Journal Series B , 41(2), p. 472.

Tomiyama, A., Tamai, H., Zun, I. & Hosokawa, S., 1999. Measurement of Transverse Migration of Single Bubbles in a Couette Flow. Pisa, 2nd Int. Symposium on Two-Phase Flow Modelling and Experimentation, p. 941.

Tomiyama, A., Tamai, H., Zun, I. & Hosokawa, S., 2002. Transverse migration of single bubbles in simple shear flows. Chemical Engineering Science , 57(11), pp. 1849-1858.

Wellek, R. M., Agrawal, A. K. & Skelland, A. H. P., 1966. Shape of Liquid Drops Moving in Liquid Media. AlChE Journal, Volume 12, p. 854.

Ziegenhein, T. & Lucas, D., 2016. On sampling bias in multiphase flows: Particle image velocimetry in bubbly flows. Flow Measurement and Instrumentation, Volume 48, pp. 36-41.

Ziegenhein, T. & Lucas, D., 2017. Observations on bubble shapes in bubble columns under different flow conditions. Experimental Thermal and Fluid Science, Volume 85, pp. 248-256.

Ziegenhein, T., Zalucky, J., Rzehak, R. & Lucas, D., 2016. On the hydrodynamics of airlift reactors, Part I: Experiments. Chemical Engineering Science, Volume 150, pp. 64-65.

Zun, I., 1980. The transverse migration of bubbles influenced by walls in vertical bubbly flow. International Journal of Multiphase Flow, Volume 6, p. 583.